



## Article

# Impact of Polymer Nanoparticles on DPPC Monolayer Properties

Alexey Bykov <sup>1,\*</sup>, Olga Milyaeva <sup>1</sup>, Alexander Akentiev <sup>1</sup>, Maria Panaeva <sup>1</sup>, Nikolaj Isakov <sup>1</sup>, Reinhard Miller <sup>2</sup> and Boris Noskov <sup>1</sup>

- <sup>1</sup> Institute of Chemistry, St. Petersburg State University, Universitetsky pr. 26, 198504 St. Petersburg, Russia; o.milyaeva@spbu.ru (O.M.); a.akentiev@spbu.ru (A.A.); st068796@student.spbu.ru (M.P.); st055657@student.spbu.ru (N.I.); b.noskov@spbu.ru (B.N.)
- <sup>2</sup> Physics Department, Technical University Darmstadt, Hochschulstraße 8, D-64289 Darmstadt, Germany; miller@fkp.tu-darmstadt.de
- \* Correspondence: ag-bikov@mail.ru

**Abstract:** The application of surface rheology and Brewster angle microscopy on mixed monolayers of DPPC and polymeric nanoparticles (cationic and anionic) showed that the sign of the particle charge affects the dynamic properties of the monolayers less than the nanoparticles' ability to aggregate. Under almost physiological conditions, the effect of nanoparticles on the elasticity of DPPC monolayer is insignificant. However, the particles prevent the surface tension from decreasing to extremely low values. This effect could affect the functionality of pulmonary surfactants.

**Keywords:** DPPC; nanoparticles; surface rheology; Langmuir monolayers



**Citation:** Bykov, A.; Milyaeva, O.; Akentiev, A.; Panaeva, M.; Isakov, N.; Miller, R.; Noskov, B. Impact of Polymer Nanoparticles on DPPC Monolayer Properties. *Colloids Interfaces* **2022**, *6*, 28. <https://doi.org/10.3390/colloids6020028>

Academic Editor: Younjin Min

Received: 17 March 2022

Accepted: 21 April 2022

Published: 26 April 2022

**Publisher's Note:** MDPI stays neutral with regard to jurisdictional claims in published maps and institutional affiliations.



**Copyright:** © 2022 by the authors. Licensee MDPI, Basel, Switzerland. This article is an open access article distributed under the terms and conditions of the Creative Commons Attribution (CC BY) license (<https://creativecommons.org/licenses/by/4.0/>).

## 1. Introduction

Lung surfactants, consisting of a mixture of lipids and proteins, play a key role in the respiratory process due to their ability of effectively reducing the surface tension to extremely low values [1,2]. Moreover, pulmonary surfactant films on the alveoli surface act as the first barrier to various pathogens and particles entering the body during respiration [3,4]. In particular, the SARS-CoV-2 coronavirus entering the lungs can disrupt the type II alveolar epithelium cells that produce pulmonary surfactants [5]. It should be noted that with the deterioration of the environmental situation and widespread use of nanoparticles in various fields of human life, the risk of lung pathologies increases [6,7]. Another reason for the interest in the compositions of pulmonary surfactants and particles of various chemical natures is associated with their use for targeted drug delivery [8–11]. Kim et al. proposed the use of polymer particles for the development of synthetic analogues of lung surfactants [12] since particles can also reduce the surface tension to very low values.

For the physical modeling of pulmonary surfactant properties, relatively simple systems [13–17] are usually used. One such system consists of monolayers of DPPC (dipalmitoylphosphatidylcholine), which are the main component of the pulmonary surfactant [18–20]. The surface tension can change when particles enter the lipid monolayer, leading to changes in the composition and structure of the surface layer. Along with the surface tension, the dynamic surface elasticity is often measured. It characterizes the behavior of the monolayer during periodic expansions and compressions [14,17,21–23]. Various types of microscopies are also used to study the structure of surface layers [24–28]. Hydrophobic nano- and microparticles strongly influence the surface properties of the lung surfactant [29]. This influence depends on the ability of particles to aggregate in the surface layer [23,30].

Most of the published works consider the effect of particles on lipid monolayers in the region of high surface tension, while much lower values of surface tension are achieved in the lungs [14,21]. This paper presents the results of the measurements of surface properties under a wide range of surface pressures, including values characteristic of the pulmonary

alveoli. Studies of the dynamic properties of a DPPC monolayer were carried out with the addition of two types of polystyrene particles with different signs of the surface charge. Since DPPC is a zwitterionic lipid, we can expect a different behavior of mixed monolayers with cationic and anionic particles.

## 2. Materials and Methods

DPPC, with a molecular weight of 734.1 D and 99% purity (Sigma-Aldrich, Darmstadt, Germany), was used as received. DPPC was diluted in chloroform at a concentration of 1 mg/mL for spreading onto the aqueous subphase.

Two samples of aqueous dispersions of polystyrene (PS) particles were provided from Molecular Probes, Eugene, OR, USA. The concentration of anionic particles with sulfate functional groups (PSA) was 8% *w/v* ( $2.1 \times 10^{16}$  particles/mL), while the concentration of cationic particles with amidine functional groups (PSC) was 4% *w/v* ( $6.3 \times 10^{15}$  particles/mL). All dispersions had no surfactant impurities. The mean diameters of PSA and PSC particles, as estimated by the transmission electron microscopy, were 19 and 23 nm, respectively. The PSA and PSC surface charge densities were  $2.4 \mu\text{C}/\text{cm}^2$  ( $6.8 \text{ nm}^2$  per one charged group) and  $3.0 \mu\text{C}/\text{cm}^2$  ( $5.4 \text{ nm}^2$  per one charged group), respectively (Molecular Probes). The zeta potentials of PSA particles in solution at pH 7 and at concentrations of NaCl 0.01 and 0.1 M NaCl were  $-64.7 (\pm 1.8)$  and  $-43.1 (\pm 2.0)$  mV, respectively. The zeta potential of the PSC particles at pH 3 and at a concentration of NaCl 0.01 M was  $+50.6 (\pm 2.7)$  mV, and at pH 7 at a concentration of NaCl 0.1 M, it was  $+23.4 (\pm 1.0)$  mV. Before spreading at the water/air interface, the PSA and PSC dispersions were diluted by 20 and 10 times, respectively, mixed with isopropyl alcohol at a volume ratio of 1:2 and subjected to ultrasonification. The volume of the Langmuir trough was around 300 mL and the addition of few microliters of isopropanol did not change the surface tension of the aqueous phase. Therefore, we assume, that isopropanol does not influence the properties of the particle monolayer.

The purification of isopropyl alcohol (Sigma-Aldrich, Germany) was made by distillation. Sodium chloride (Sigma-Aldrich, Germany) was calcined at about 750 °C for several hours to remove any organic impurities. For all experiments, the water was deionized using a multicartridge system (Direct-Q). The lipid monolayers were spread onto the sodium chloride solutions subphase in a PTFE Langmuir trough by a microsyringe (Hamilton, Switzerland). After the spreading of the lipid solution, the PS particle dispersion in the water/isopropyl alcohol mixture was spread onto the liquid surface to prepare a mixed monolayer with the required surface concentration. The surface concentration was calculated on the basis of the area occupied by pure monolayers of both components in the most compressed state before collapse. In this work, mixed monolayers of DPPC and PS nanoparticles were studied with the area ratios of the two components of 1:1 or 10:1, respectively. For example, at a ratio of 1:1, the area filled by closely packed lipid molecules was equal to the area filled by closely packed PS particles. With this ratio of DPPC and PS areas, the weight ratio of the monolayer components was 1:200, respectively. To ensure equilibrium conditions and solvent evaporation after spreading, the measurements were started one hour after the formation of the monolayer.

The oscillating barrier method was used in the range of high surface tensions to measure the dynamic dilational surface elasticity. In our equipment—the Interface Shear Rheometer (KSV NIMA, Espoo, Finland)—two symmetrically moving PTFE barriers induced low-frequency oscillations of the monolayer area in a PTFE Langmuir trough. The corresponding surface tension oscillations were measured by the Wilhelmy plate method using a filter paper plate with a width of 1 cm and was positioned parallel to the barriers in the center of the through. The area between the PTFE barriers before oscillations was  $75 \times 150 \text{ mm}^2$ . The amplitude of area oscillations ( $\pm 2\%$ ) and the frequency of 0.03 Hz were kept constant in all experiments. At this frequency of surface area oscillations, the behavior of the surface layer proved to be almost purely elastic, and the real part of surface elasticity almost coincided with the elasticity modulus, while the imaginary part was close to zero. Therefore, we discuss only the modulus of surface elasticity. This standard procedure for

measurements of the dynamic surface elasticity using a Langmuir trough can be applied only in the range of relatively low surface pressures (below 50 mN/m) due to the possible leakage of surfactants molecules from the area between the barriers at extremely low surface tensions.

The modified stress decomposition method [31–34] was used for the determination of the effective surface elasticity in the range of low surface tensions of spread monolayer (about 32 mN/m). According to this approach the comparison of system responses (increments of surface tension) at different surface deformations allows the determination of the surface elasticity [31,32]. In this case, the effective dynamic surface elasticity in the compressed ( $\epsilon'_{ef}$ ) and expanded ( $\epsilon''_{ef}$ ) states is calculated from the difference in the system responses for two given deformations [31,33]. From the difference of the surface tension responses ( $\Delta\gamma'$ ) or ( $\Delta\gamma''$ ), which correspond to the deformation amplitudes  $\Delta A^1$  and  $\Delta A^2$ , the effective surface elasticity value,  $\epsilon_{ef}$ , can be determined.

Brewster angle microscopy (BAM-1 set-up, Nanofilm, Germany) was used to visualize the monolayer morphology.

### 3. Results and Discussion

#### 3.1. Nanoparticle Layers

This section describes the results of the monolayers of particles without DPPC. First, the properties of the deposited layer of cationic nanoparticles were determined, since only monolayers of anionic particles had previously been studied in detail [35,36]. Unlike anionic particles with sulfate groups, the charge of cationic particles depends on the pH of the medium. To compare our results from the cationic particles with the data from the anionic particles, the cationic particles were spread onto a subphase of hydrochloric acid with a pH 3, where all functional groups were ionized. At the same time, monolayers of anionic particles were deposited onto a subphase with a pH 7.

During compression, the increase of the surface concentration of cationic particles led to a gradual increase of the surface pressure and elasticity (Figure 1, Figures S1 and S2). The ionic strength of the monolayer subphase strongly influenced the absolute values of the surface elasticity and the  $|\epsilon|(\pi)$  dependence of surface elasticity on the surface pressure for the spread monolayers of nanoparticles. The ionic strength of the solution was controlled by adding sodium chloride. When the monolayer was deposited onto a 0.01 M NaCl solution, the surface elasticity gradually increased to about 100 mN/m as the surface pressure increased to 30 mN/m (Figure 1). With further compression, the surface pressure almost did not change, which indicated the collapse of the deposited film.

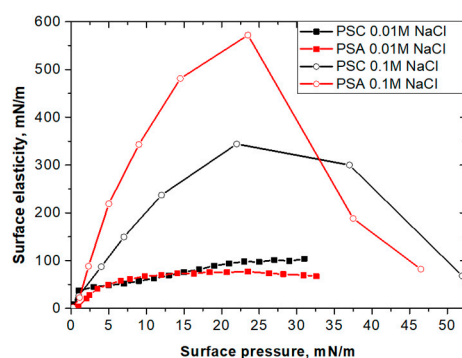


**Figure 1.** Dependencies of the surface elasticity modulus on surface pressure for spread cationic (black symbols) and anionic (red symbols) PS nanoparticles on the surface of 0.01 M (filled symbols) and 0.1 M (unfilled symbols) NaCl solutions.

At higher ionic strength (0.1 M NaCl) the surface pressure of the spread nanoparticle monolayer increased to about 72 mN/m upon compression (Figures S1 and S2). Therefore, the surface tension turned out to be close to 0. In this case, the dependence of surface elasticity on surface pressure passed through a maximum ( $\sim 300$  mN/m). Such behavior

was previously observed for deposited monolayers of anionic nanoparticles [35–37]. At low ionic strength, the nanoparticles are in a non-aggregated state due to strong electrostatic repulsion, which can lead to an elasticity increase of up to 100 mN/m. In this case, the surface film collapsed due to the displacement of individual particles from the surface into the bulk under strong compression and surface pressures above 30 mN/m [36]. At a salt concentration in the subphase of 0.1 M NaCl, the electrostatic interaction between the particles was mainly shielded and resulted in a two-dimensional particle aggregation due to capillary attraction forces (Figure 1). These aggregates began to interact with each other upon compression, leading to the increase in surface elasticity and pressure to very high values (more than 100 mN/m), i.e., close to the values observed for the monolayers of microparticles [35]. Although the collapse pressure equaled the surface tension of the aqueous subphase, the surface elasticity approached zero at much lower surface pressures (measured by the Wilhelmy plate), due to the surface tension gradient along the surface (Figure 1). It was shown previously that the apparent critical surface pressure corresponding to the collapse depended on the particle surface concentration, due to the development of a surface tension gradient near the moving barriers over the course of compression [35]. The critical surface pressure at the beginning of the collapse, i.e., at an abrupt decrease in the slope of the surface pressure isotherm, varied depending on the different amounts of particles in the spread monolayer (Figure S3).

These findings are supported by Brewster angle microscopy data (Figure 2). At low ionic strength, individual macroscopic two-dimensional phases cannot be observed (Figure 2b). However, at higher ionic strength, microscopic two-dimensional regions with clear boundaries are observed immediately after particle deposition (Figure 2a). Similar results were obtained for films of anionic particles.

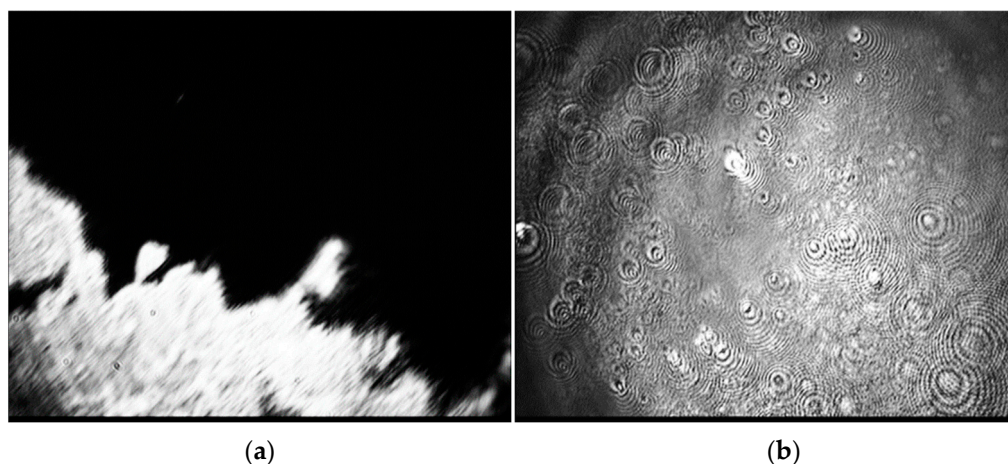


**Figure 2.** BAM-images of monolayers of spread cationic polystyrene nanoparticles onto a NaCl subphase with a NaCl concentration of 0.1 M (a) and 0.01 M (b). The surface pressure is zero. (Image size is around 1 mm × 0.8 mm).

### 3.2. Mixed Films of Nanoparticles and DPPC at High Surface Tensions

This section describes the results for mixed monolayers of particles and DPPC at surface pressures below 50 mN/m. Measurements of the dynamic surface properties for mixed monolayers of DPPC and particles correspond to pH 3 of the subphase for cationic particles and pH 7 for anionic particles. When the pH of the subphase was changed from 7 to 3, the properties of a DPPC monolayer remained almost unchanged. When the surface pressure increased, the surface elasticity initially increased too. At surface pressures close to 10 mN/m, a minimum of the elasticity was observed. It could be assumed that it is associated with a two-dimensional phase transition [32,38]. Further compression resulted in an elasticity increase of up to 300 mN/m, which corresponds to a close-packed monolayer. The properties of mixed DPPC monolayers with cationic and anionic nanoparticles were measured with

three sets of main parameters. First: the area ratio between DPPC and particle coverages was 1 to 1, and the ionic strength was 0.01 M. Second: the area ratio between DPPC and particle coverages was 1 to 1, and the ionic strength was 0.1 M. Third: the area ratio between DPPC and particle coverages was 10 to 1, and the ionic strength was 0.01 M.

DPPC is a zwitterionic lipid and can exhibit some specificity for interactions with particles of different sign in the surface charge. However, the performed studies of mixed DPPC monolayers with cationic and anionic nanoparticles have shown that in the region of relatively high surface tensions ( $>30$  mN/m), the charge sign of the particles effects the dynamic surface properties only slightly (Figure 3).

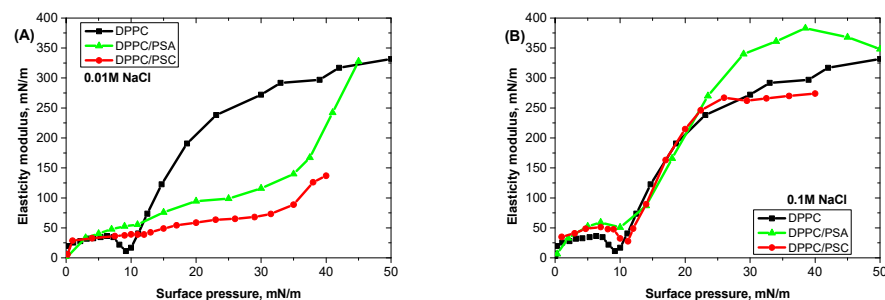


**Figure 3.** Dependences of the surface elasticity modulus on surface pressure for spread DPPC monolayers (black squares), mixed monolayers of DPPC with anionic (green triangles) or cationic (red circles) PS nanoparticles onto the subphase of NaCl solution with concentrations of 0.01 M (A) and 0.1 M (B). The approximate ratio of DPPC to nanoparticles surface coverage is 1:1.

At a high concentration of non-aggregated particles (0.01 M NaCl subphase), the minimum dependence of the surface elasticity on the surface pressure disappeared. The surface elasticity at surface pressures of 12 to 25 mN/m also decreased remarkably for mixed monolayers as compared to the pure lipid monolayer (Figure 3A). The change of the surface elasticity dependence is caused by changes in the surface layer structure in presence of non-aggregated nanoparticles. Separate nanoparticles prevent the formation of a homogeneous close-packed liquid-condensed lipid phase [39,40] (Figure 4A). In this case, a noticeable increase in surface elasticity is observed only at surface pressures above 30 mN/m.

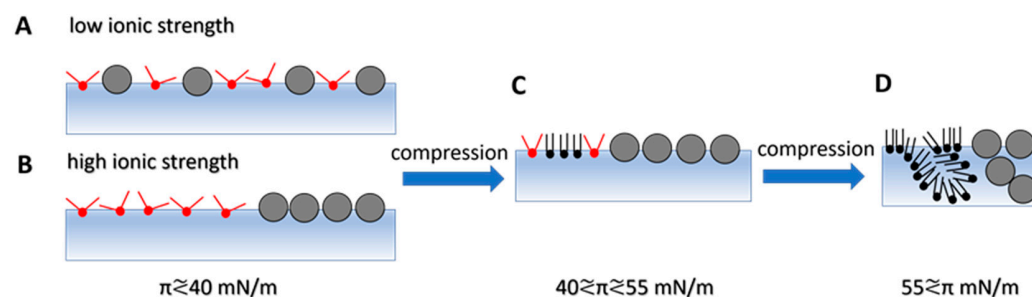


**Figure 4.** Scheme of the structure of DPPC and polystyrene particles mixed monolayers at liquid-gas interface in a wide range of surface pressures. The approximate ratio of DPPC to nanoparticles surface coverage is 1:1. See description in the text.

Previously, it has been shown that the compression of mixed monolayers of anionic nanoparticles in the presence of DPPC leads to an increase in surface pressure above 30 mN/m, resulting in an irreversible two-dimensional aggregation of nanoparticles in the surface layer [23]. Due to the influence of the lipid, the collapse mechanism for nanoparticles changes. Instead of the displacement of individual particles from the surface, a particle aggregation occurs in presence of lipid. This process is associated with surface tension changes at the liquid-gas interface [23]. As the mixed monolayer is compressed, the surface tension in the area between particles decreases. As a result, the contact angle of the particles also changes, leading to the formation of two-dimensional aggregates. The increase of



the area occupied by a two-dimensional aggregate compared to the area occupied by an individual particle leads to a significant increase of energy needed to remove particles from the surface. At a high ionic strength (0.1 M NaCl), the aggregation of nanoparticles occurs immediately after spreading. In this case, the particles' influence on the DPPC monolayer properties is noticeably weaker than in the previous case (Figure 3B). The dependences of the surface elasticity show a small minimum in the region of the two-dimensional phase transition and a noticeable elasticity increase at average surface pressures. Such behavior is similar to that of a pure DPPC monolayer.

This situation could be explained by assuming that the particles interact only slightly with the lipid molecules since the contact between the two components occurs only along the edge of the two-dimensional particle aggregates (Figure 4B). The similarity of the surface elasticity dependences for mixed monolayers with cationic and anionic particles indicates that for both types of particles the same aggregation process takes place. A similar influence of cationic and anionic nanoparticles on the properties of DPPC monolayers is confirmed by the close compression isotherms for these two systems (Figure S4).

The increase of the lipid surface concentration (when the ratio between the components is changed from 1:1 to 10:1) and the corresponding decrease of the particles fractional coverage also leads to a decrease of particles' influence (Figure 5). In this case, even for particles in a non-aggregated state, the dependences of the surface elasticity for pure DPPC and the mixed monolayer almost coincide. Only at surface pressures of about 20 mN/m there is a slight decrease in the elasticity in the presence of particles. It is probably the case that the number of particles is not enough to disrupt the structure of the lipid monolayer.

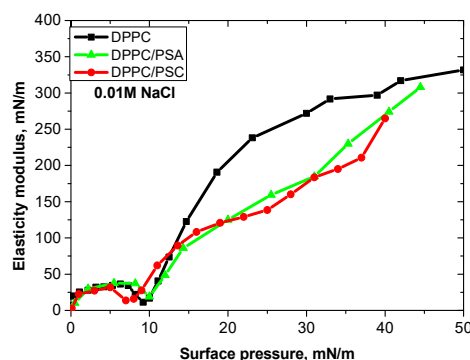


**Figure 5.** Dependences of the surface elasticity on surface pressure for the spread DPPC monolayers (black squares), mixed with anionic (green triangles) or cationic (red circles) PS nanoparticle monolayers on a NaCl subphase with a concentration of 0.01 M. The approximate area ratio of DPPC molecules to nanoparticles in the surface layer is 10:1.

### 3.3. Mixed Films of Nanoparticles and Lipid at Low Surface Tensions

In order to measure the effective surface elasticity in the region of high surface pressures (low surface tensions) at the liquid–gas interface, a monolayer with a surface pressure of about 40 mN/m was formed by sequential deposition and the compression of the surface. Furthermore, the monolayer was subjected to harmonic deformations with different amplitudes [32]. This approach was applied first to monolayers of pure DPPC and then to mixed monolayers of DPPC and polystyrene particles. The dynamic surface properties of pure DPPC monolayers in the region of extremely low surface tensions have previously been discussed in detail [32,41].

When the surface pressure increases to around 40–45 mN/m, the surface elasticity reaches high values due to the formation of highly ordered structures of the DPPC monolayer (Figures 5 and 6). Under further compression the layer becomes heterogeneous. The heterogeneity leads to an additional mechanism of the surface stress relaxation and, as a consequence, to a surface elasticity decrease (Figure 6). The formation of inhomogeneities in a DPPC monolayer at high surface pressures has been observed in many studies using atomic force microscopy [42,43]. Despite the appearance of surface layer heterogeneities,

the effective surface elasticity of the DPPC monolayer exceeds 100 mN/m until the surface pressure reaches about 72 mN/m, which corresponds to an almost zero surface tension.

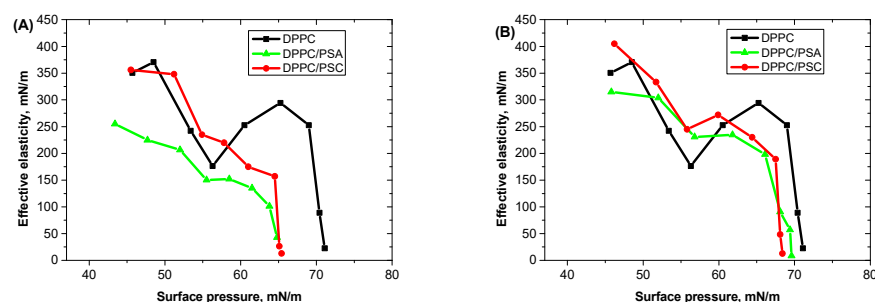


**Figure 6.** Dependences of the effective surface elasticity on surface pressure for spread DPPC monolayers (black squares), mixed monolayers of DPPC with anionic (green triangles) or cationic (red circles) PS nanoparticles, respectively, on the phosphate buffer solution at pH of 7.4 and at a NaCl concentration of 0.1 M. The approximate area ratio of DPPC molecules to nanoparticles is 1:1 (A) and 10:1 (B), respectively.

In this study, the effect of anionic and cationic nanoparticles on the properties of DPPC monolayers under almost physiological conditions was studied for the first time. For this purpose, the measurements were carried out at a high ionic strength of the subphase and in the region of high surface pressures. At the surface of a phosphate buffer at pH 7 and a NaCl concentration of 0.1 M, the mixed monolayers of lipid and nanoparticles were formed by the sequential spreading of the components. Although the solution ionic strength at physiological conditions is around 0.15 M, in this study the results relate to a slightly lower ionic strength with the aim of comparison with the data for particle monolayers without lipids. We can expect that the ionic strength increase does not affect the surface properties significantly, since the electrostatic repulsion between the particles was already screened at an ionic strength of 0.1 M.

The effective surface elasticity was measured close to the surface tension values inside the lungs [32,33]. At high ionic strength of the subphase and low surface tension, both cationic and anionic particles are in an aggregated state. As it was shown above, such aggregates are characterized by a high surface elasticity.

The obtained results for mixed monolayers of DPPC and nanoparticles can be divided into three groups, depending on the surface pressure: about 40 mN/m, from 40 to 50–55 mN/m, and above 55 mN/m.

At surface pressures of about 40 mN/m, even at high particle surface concentrations, the surface elasticity remains high (Figure 6A). This is in a good agreement with previously obtained results for monolayers of pure components which have a high (above 200 mN/m) elasticity at such a surface pressure. The interaction between the components in the surface layer is presumably weak at  $\pi = 40$  mN/m (Figure 4C). The further surface compression (surface pressure increase above 40 mN/m) leads to a decrease of the surface elasticity. It can be associated not only with the changes in the DPPC monolayer structure, but also with the changes in the structure of nanoparticle aggregates. The decrease of the surface tension at the liquid–gas interface also changes the wetting angle of the particles [36]. It was shown previously that the surface tension decreases from 72 to 21 mN/m during the transition from an air–water to an oil–water interface, which resulted in a decrease of the surface elasticity of a particle monolayer from 300 mN/m to 100 mN/m [36]. Thus, it can be assumed that the surface elasticity becomes lower at a surface pressure increase from 40 to 50–55 mN/m due to combined effects of the lipid parts of the monolayer and the particle aggregates.

The third group of results relates to surface pressures above 55 mN/m (Figure 4D). In this region, the dynamic surface elasticity of mixed monolayers drops sharply to almost zero (Figure 6). The minimum surface tension at a compression of mixed monolayers differs

from the corresponding values for pure DPPC monolayer. At high concentrations of the particles, the minimum surface tension for a mixed monolayer increases as compared to that for a pure DPPC monolayer. The minimum value increases from 0.5 mN/m for a pure DPPC monolayer to 7 mN/m for mixed monolayers. This effect may be a consequence of changes in the structure of the mixed layer comprised of DPPC and particles. Under strong compression and at low surface tensions, the particles can be displaced from the surface, even if they are aggregated. The energy required to remove the particles from the surface depends not only on the occupied area, but also on the surface tension at the air–water interface between the particles [44]. The lower the surface tension, the easier the particles can be displaced from the surface, and this process becomes possible even for the particle aggregates. When the surface tension at the air–water interface between particles decreases significantly, due to the increase in the local concentration of DPPC molecules, the energy required to remove particles or their aggregates is significantly reduced. As a result, during compression, some particle aggregates may be displaced from the surface. The formation of a three-dimensional structure in a mixed monolayer can lead to a sharp decrease in the effective surface elasticity down to zero.

At the same time, the particle displacement is incomplete and/or reversible. Brewster angle microscopy shows that some particles are still visible at the surface at minimum surface tension values (Figure 7). As the surface concentration of particles decreases, their influence on the minimum surface tension values of the mixed monolayer decreases (Figure 6B). When the surface concentration of particles is ten times less than the DPPC concentration, the minimum surface tension values increase from 0.5 mN/m to about 3 mN/m for the mixed monolayer.

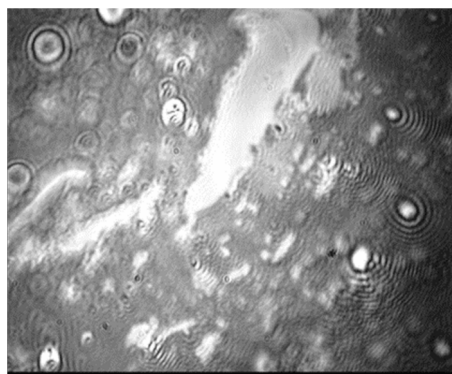


**Figure 7.** BAM-image of a mixed monolayer of DPPC/PSA particles at the surface of a 0.1 M NaCl solution after a few surface compression–expansion cycles. The surface pressure is around 30 mN/m. (Image size is 1 mm × 0.8 mm).

The ability of pulmonary surfactant to reduce the surface tension to almost zero values prevents the collapse of the alveoli during exhalation and defines many functional properties of the lungs. Therefore, the increase of the minimum surface tension values due to the presence of particles on the surface of the lungs could have a negative effect and could lead to various diseases. It should be noted that the increase of the minimal surface tension depends on the concentration of particles in the surface layer. According to the obtained results, a significant increase in the minimal surface tension was observed for sufficiently high surface concentrations of the nanoparticles in mixed monolayers. When particles occupy only a small surface area, their influence on the minimal surface tension in a compressed state of pulmonary surfactants may be negligible.

#### 4. Conclusions

The investigation of the spread monolayers of cationic and anionic polymeric nanoparticles shows that, regardless of the sign of the charge, their behavior in the surface layer is similar. The ionic strength of the subphase and the surface tension at the air–water interface determines the tendency of the particles to aggregate and also the properties of mixed



monolayers in the region of relatively high surface tensions (up to 30 mN/m). At low ionic strength and relatively low surface pressures, the particles do not aggregate in the surface layer. Such separate nanoparticles prevent the formation of densely packed DPPC layers with a high elasticity more effectively than the large particle aggregates.

Under conditions close to the physiological state within the lungs (surface pressures of about 40 mN/m and a high ionic strength of the substrate), nanoparticles are aggregated and have only a slight effect on the dynamic surface elasticity of DPPC monolayers. However, the presence of particles in DPPC monolayers prevents the surface tension from dropping to extremely low values upon compression. This drop is observed in lung surfactants and pure DPPC monolayers and is considered one of the key factors of the pulmonary surfactant's functionality. Therefore, nanoparticles can lead to an impaired functionality of pulmonary surfactants.

**Supplementary Materials:** The following supporting information can be downloaded at: <https://www.mdpi.com/article/10.3390/colloids6020028/s1>, Figure S1: Compression isotherms of PSA nanoparticles at the surface of 0.01 M (black circles) and 0.1 M (red squares) NaCl solutions; Figure S2: Compression isotherms of PSC nanoparticles at the surface of 0.01 M (black circles) and 0.1 M (red squares) NaCl solutions; Figure S3: Compression isotherms for PSA microparticles (with diameter 1  $\mu\text{m}$ ) on the surface of 0.01M NaCl solution when 200  $\mu\text{L}$  (black squares) and 400  $\mu\text{L}$  (red circles) of the dispersion were spread at the air-water interface; Figure S4: Compression isotherms for pure DPPC (open black squares), DPPC/PSA (red circles) and DPPC/PSC (green triangles) monolayers at the surface 0.1M NaCl. The approximate ratio of DPPC to nanoparticles surface coverage is 1:1.

**Author Contributions:** Supervision, B.N.; conceptualization, A.B.; methodology, A.A.; investigation, A.B., M.P. and N.I.; writing—original draft preparation, A.B., O.M. and B.N.; writing—review, R.M. All authors have read and agreed to the published version of the manuscript.

**Funding:** The study was financially supported by the Russian Science Foundation (project 22-23-00235).

**Institutional Review Board Statement:** Not applicable.

**Informed Consent Statement:** Not applicable.

**Data Availability Statement:** Not applicable.

**Acknowledgments:** A.B., O.M., A.A., M.P., and N.I. would like to thank our mentor, Boris A. Noskov, for the patient guidance, encouragement and advice he has provided throughout our work and life. The authors are grateful to the Center for Optical and Laser Materials, Thermogravimetric and Calorimetric Research Centre, and the Centre for Microscopy and Microanalysis of St. Petersburg State University for the assistance in the investigation.

**Conflicts of Interest:** The authors declare no conflict of interest.

## References

1. Echaide, M.; Autilio, C.; Arroyo, R.; Perez-Gil, J. Restoring pulmonary surfactant membranes and films at the respiratory surface. *Biochim. Biophys. Acta Biomembr.* **2017**, *9*, 1725–1739. [[CrossRef](#)] [[PubMed](#)]
2. Castillo-Sanchez, J.C.; Cruz, A.; Perez-Gil, J. Structural hallmarks of lung surfactant: Lipid-protein interactions, membrane structure and future challenges. *Arch. Biochem. Biophys.* **2021**, *703*, 108850. [[CrossRef](#)] [[PubMed](#)]
3. Sosnowski, T.R. Inhaled aerosols: Their role in COVID-19 transmission, including biophysical interactions in the lungs. *Curr. Opin. Colloids Interface Sci.* **2021**, *54*, 101451. [[CrossRef](#)]
4. Guzmán, E.; Santini, E. Lung surfactant models and particles at fluid interfaces: Making preliminary toxicity assessments of inhaled particles. *Curr. Opin. Colloids Interface Sci.* **2019**, *39*, 24–39. [[CrossRef](#)]
5. Zuo, Y.Y.; Uspal, W.E.; Wei, T. Airborne transmission of COVID-19: Aerosol dispersion, lung deposition, and virus-receptor interactions. *ACS Nano* **2020**, *14*, 16502–16524. [[CrossRef](#)]
6. Schleh, C.; Hohlfeld, J.M. Interaction of nanoparticles with the pulmonary surfactant system. *Inhal. Toxicol.* **2009**, *21*, 97–103. [[CrossRef](#)]
7. Guzmán, E.; Santini, E.; Ferrari, M.; Liggieri, L.; Ravera, F. Evaluating the impact of hydrophobic silicon dioxide in the interfacial properties of lung surfactant films. *Environ. Sci. Technol.* **2022**; *in press*. [[CrossRef](#)]
8. Gregory, T.J.; Steinberg, K.P.; Spragg, R.; Gadek, J.E.; Hyers, T.M.; Longmore, W.J.; Moxley, M.A.; Cai, G.Z.; Hite, R.D.; Smith, R.M.; et al. Bovine surfactant therapy for patients with acute respiratory distress syndrome. *Am. J. Respir. Crit. Care Med.* **1997**, *155*, 1309–1315. [[CrossRef](#)]

9. Veldhuizen, R.A.W.; Zuo, Y.Y.; Petersen, N.O.; Lewis, J.F.; Possmayer, F. The COVID-19 pandemic: A target for surfactant therapy? *Expert Rev. Respir. Med.* **2021**, *15*, 597–608. [[CrossRef](#)] [[PubMed](#)]
10. Baer, B.; Souza, L.M.P.; Pimentel, A.S.; Veldhuizen, R.A.W. New insights into exogenous surfactant as a carrier of pulmonary therapeutics. *Biochem. Pharmacol.* **2019**, *164*, 64–73. [[CrossRef](#)]
11. Hidalgo, A.; Cruz, A.; Pérez-Gil, J. Barrier or carrier? Pulmonary surfactant and drug delivery. *Eur. J. Pharm. Biopharm.* **2015**, *95*, 117–127. [[CrossRef](#)]
12. Kim, H.C.; Suresh, M.V.; Singh, V.V.; Arick, D.Q.; Machado-Aranda, D.A.; Raghavendran, K.; Won, Y.Y. Polymer Lung Surfactants. *ACS Appl. Bio Mater.* **2018**, *1*, 581–592. [[CrossRef](#)]
13. Sosnowski, T.R. Particles on the lung surface—Physicochemical and hydrodynamic effects. *Curr. Opin. Colloids Interface Sci.* **2018**, *36*, 1–9. [[CrossRef](#)]
14. Sosnowski, T.R.; Kubski, P.; Wojciechowski, K. New experimental model of pulmonary surfactant for biophysical studies. *Colloids Surf. A* **2017**, *519*, 27–33. [[CrossRef](#)]
15. Schüer, J.J.; Arndt, A.; Wölk, C.; Pinnapireddy, S.R.; Bakowsky, U. Establishment of a Synthetic In Vitro Lung Surfactant Model for Particle Interaction Studies on a Langmuir Film Balance. *Langmuir* **2020**, *36*, 4808–4819. [[CrossRef](#)]
16. Farnoud, A.M.; Fiegel, J. Calf lung surfactant recovers surface functionality after exposure to aerosols containing polymeric particles. *J. Aerosol Med. Pulm. Drug Deliv.* **2015**, *29*, 10–23. [[CrossRef](#)] [[PubMed](#)]
17. Guzman, E.; Ferrari, M.; Santini, E.; Liggieri, L.; Ravera, F. Effect of silica nanoparticles on the interfacial properties of a canonical lipid mixture. *Colloids Surf. B* **2015**, *136*, 971–980. [[CrossRef](#)]
18. Farnoud, A.M.; Fiegel, J. Low concentrations of negatively charged sub-micronparticles alter the microstructure of DPPC at the air–water interface. *Colloids Surf. A* **2012**, *415*, 320–327. [[CrossRef](#)]
19. Farnoud, A.M.; Fiegel, J. Interaction of dipalmitoyl phosphatidylcholine monolayers with a particle-laden subphase. *J. Phys. Chem. B* **2013**, *117*, 12124–12134. [[CrossRef](#)]
20. Guzman, E.; Santini, E.; Ferrari, M.; Liggieri, L.; Ravera, F. Interfacial properties of mixed DPPC-hydrophobic fumed silica nanoparticle layers. *J. Phys. Chem. C* **2015**, *119*, 21024–21034. [[CrossRef](#)]
21. Ravera, F.; Miller, R.; Zuo, Y.Y.; Noskov, B.A.; Bykov, A.G.; Kovalchuk, V.I.; Loglio, G.; Javadi, A.; Liggieri, L. Methods and models to investigate the physico-chemical functionality of pulmonary surfactant. *Curr. Opin. Colloids Interface Sci.* **2021**, *55*, 101467. [[CrossRef](#)]
22. Kondej, D.; Sosnowski, T.R. Interfacial rheology for the assessment of potential health effects of inhaled carbon nanomaterials at variable breathing conditions. *Sci. Rep.* **2020**, *10*, 14044. [[CrossRef](#)]
23. Bykov, A.G.; Gochev, G.; Loglio, G.; Miller, R.; Panda, A.K.; Noskov, B.A. Dynamic surface properties of mixed monolayers of polystyrene micro- and nanoparticles with DPPC. *Colloids Surf. A Physicochem. Eng. Asp.* **2017**, *521*, 239–246. [[CrossRef](#)]
24. Xu, L.; Yang, Y.; Zuo, Y.Y. Atomic force microscopy imaging of adsorbed pulmonary surfactant films. *Biophys. J.* **2020**, *119*, 756–766. [[CrossRef](#)] [[PubMed](#)]
25. Guzman, E.; Santini, E.; Zabiegaj, D.; Ferrari, M.; Liggieri, L.; Ravera, F. Interaction of carbon black particles and dipalmitoylphosphatidylcholine at the water/air interface: Thermodynamics and rheology. *J. Phys. Chem. C* **2015**, *119*, 26937–26947. [[CrossRef](#)]
26. Finot, E.; Markey, L.; Hane, F.; Amrein, M.; Leonenko, Z. Combined atomic force microscopy and spectroscopic ellipsometry applied to the analysis of lipid-protein thin films. *Colloids Surf. B Biointerfaces* **2013**, *104*, 289–293. [[CrossRef](#)]
27. Przybyla, R.J.; Wright, J.; Parthiban, R.; Nazemidashtarjandi, S.; Kaya, S.; Farnoud, A.M. Electronic cigarette vapor alters the lateral structure but not tensiometric properties of calf lung surfactant. *Respir. Res.* **2017**, *18*, 193. [[CrossRef](#)] [[PubMed](#)]
28. Arora, S.; Kappl, M.; Haggi, M.; Young, P.M.; Traini, D.; Jain, S. An investigation of surface properties, local elastic modulus and interaction with simulated pulmonary surfactant of surface modified inhalable voriconazole dry powders using atomic force microscopy. *RSC Adv.* **2016**, *6*, 25789–25798. [[CrossRef](#)]
29. Valle, R.P.; Huang, C.L.; Loo, J.S.C.; Zuo, Y.Y. Increasing hydrophobicity of nanoparticles intensifies lung surfactant film inhibition and particle retention. *ACS Sustain. Chem. Eng.* **2014**, *2*, 1574–1580. [[CrossRef](#)]
30. Yang, Y.; Xu, L.; Dekkers, S.; Zhang, L.G.; Cassee, F.R.; Zuo, Y.Y. Aggregation state of metal-based nanomaterials at the pulmonary surfactant film determines biophysical inhibition. *Environ. Sci. Technol.* **2018**, *52*, 8920–8929. [[CrossRef](#)]
31. Bykov, A.G.; Liggieri, L.; Noskov, B.A.; Pandolfini, P.; Ravera, F.; Loglio, G. Surface dilational rheological properties in the nonlinear domain. *Adv. Colloids Interface Sci.* **2015**, *222*, 110–118. [[CrossRef](#)]
32. Bykov, A.G.; Loglio, G.; Ravera, F.; Liggieri, L.; Miller, R.; Noskov, B.A. Dilational surface elasticity of spread monolayers of pulmonary lipids in a broad range of surface pressure. *Colloids Surf. A* **2018**, *541*, 137–144. [[CrossRef](#)]
33. Bykov, A.G.; Loglio, G.; Miller, R.; Milyaeva, O.Y.; Michailov, A.V.; Noskov, B.A. Dynamic properties and relaxation processes in surface layer of pulmonary surfactant solutions. *Colloids Surf. A Physicochem. Eng. Asp.* **2019**, *573*, 14–21. [[CrossRef](#)]
34. Bykov, A.G.; Milyaeva, O.Y.; Isakov, N.A.; Michailov, A.V.; Loglio, G.; Miller, R.; Noskov, B.A. Dynamic properties of adsorption layers of pulmonary surfactants. Influence of matter exchange with bulk phase. *Colloids Surf. A* **2021**, *611*, 125851. [[CrossRef](#)]
35. Bykov, A.G.; Noskov, B.A.; Loglio, G.; Lyadinskaya, V.V.; Miller, R. Dilational surface elasticity of spread monolayers of polystyrene microparticles. *Soft Matter* **2014**, *10*, 6499–6505. [[CrossRef](#)] [[PubMed](#)]
36. Bykov, A.G.; Loglio, G.; Miller, R.; Noskov, B.A. Dilational surface elasticity of monolayers of charged polystyrene nano- and microparticles at liquid/fluid interfaces. *Colloids Surf. A Physicochem. Eng. Asp.* **2015**, *485*, 42–48. [[CrossRef](#)]

37. Noskov, B.A.; Bykov, A.G. Dilational rheology of monolayers of nano- and microparticles at the liquid-fluid interfaces. *Curr. Opin. Colloids Interface Sci.* **2018**, *37*, 1–12. [[CrossRef](#)]
38. Wüstneck, R.; Perez-Gil, J.; Wüstneck, N.; Cruz, A.; Fainerman, V.B.; Pison, U. Interfacial properties of pulmonary surfactant layers. *Adv. Colloids Interface Sci.* **2005**, *117*, 33–58. [[CrossRef](#)]
39. Guzman, E.; Orsi, D.; Cristofolini, L.; Liggieri, L.; Ravera, F. Two-dimensional DPPC based emulsion-like structures stabilized by silica nanoparticles. *Langmuir* **2014**, *30*, 11504–11512. [[CrossRef](#)]
40. Orsi, D.; Guzmán, E.; Liggieri, L.; Ravera, F.; Ruta, B.; Chushkin, Y.; Rimoldi, T.; Cristofolini, L. 2D dynamical arrest transition in a mixed nanoparticle-phospholipid layer studied in real and momentum spaces. *Sci. Rep.* **2015**, *5*, 17930. [[CrossRef](#)]
41. Bykov, A.G.; Guzmán, E.; Rubio, R.G.; Krycki, M.M.; Milyaeva, O.Y.; Noskov, B.A. Influence of temperature on dynamic surface properties of spread DPPC monolayers in a broad range of surface pressures. *Chem. Phys. Lipids* **2019**, *225*, 104812. [[CrossRef](#)] [[PubMed](#)]
42. Zuo, Y.Y.; Veldhuizen, R.A.; Neumann, A.W.; Petersen, N.O.; Possmayer, F. Current perspectives in pulmonary surfactant-inhibition, enhancement and evaluation. *Biochim. Biophys. Acta* **2008**, *1778*, 1947–1977. [[CrossRef](#)] [[PubMed](#)]
43. Liekkinen, J.; Enkavi, G.; Javanainen, M.; Olmeda, B.; Perez-Gil, J.; Vattulainen, I. Pulmonary surfactant lipid reorganization induced by the adsorption of the oligomeric surfactant protein B complex. *J. Mol. Biol.* **2020**, *432*, 3251–3268. [[CrossRef](#)] [[PubMed](#)]
44. Binks, B.P. Particles as surfactants similarities and differences. *Curr. Opin. Colloids Interface Sci.* **2002**, *7*, 21–41. [[CrossRef](#)]